Imaging of N-Linked Glycans in Biological Tissue Sections using Nanospray Desorption Electrospray Ionization (nano-DESI) Mass Spectrometry

Miranda R. Weigand[1], Alyssa M. Moore[1], Hang Hu[1], Peggi M. Angel[2], Richard R. Drake[2], and Julia Laskin[1*]

[1]Department of Chemistry, College of Science, Purdue University, West Lafayette, IN 47907

[2]Department of Cell and Molecular Pharmacology and Experimental Therapeutics, Medical University of South Carolina, Charleston, SC 29425

Abstract

N-linked glycans are complex biomolecules vital to cellular functions that have been linked to a wide range of pathological conditions. Mass spectrometry imaging (MSI) has been used to study the localization of N-linked glycans in cells and tissues. However, their structural diversity presents a challenge for MSI techniques, which stimulates the development of new approaches. In this study, we demonstrate for the first time spatial mapping of N-linked glycans in biological tissues using nanospray desorption electrospray ionization mass spectrometry imaging (nano-DESI MSI). Nano-DESI MSI is an ambient ionization technique that has been previously used for imaging of metabolites, lipids, and proteins in biological tissue samples without special sample pretreatment. N-linked glycans are released from glycoproteins using an established enzymatic digestion with peptide N-glycosidase F and their spatial localization is examined using nano-DESI MSI. We demonstrate imaging of N-linked glycans in formalin-fixed paraffin-embedded human hepatocellular carcinoma and human prostate tissues in both positive and negative ionization modes. We examine the localization of 38 N-linked glycans consisting of high mannose, hybrid fucosylated, and sialyated glycans. We demonstrate that negative mode nano-DESI MSI is well-suited for imaging of underivatized sialylated N-linked glycans. On-tissue MS/MS of different adducts of N-linked glycans proves advantageous for elucidation of the glycan sequence. This study demonstrates the applicability of liquid extraction techniques for spatial mapping of N-linked glycans in biological samples, providing an additional tool for glycobiology research.

Keywords: N-linked glycans, nano-DESI, mass spectrometry imaging, hepatocellular carcinoma, prostate cancer

Introduction

Glycosylation is a widespread post-translational modification of proteins that affects their stability, folding, and interactions and plays an essential role in biological processes such as cell signaling and signal transduction.[1–3] N-linked glycans are oligosaccharides covalently attached to asparagine (Asn) residues of proteins containing the Asn-X-Ser/Thr consensus sequence, in which "X" is any amino acid except for proline. Their structural diversity and complexity present a challenge to both qualitative and quantitative analysis of biological samples with existing analytical techniques. At present, the most common technique for studying N-linked glycans is liquid chromatography-mass spectrometry (LC-MS).[4] LC-MS has been used for confident characterization and quantitation of complex glycan mixtures with the drawback of extensive sample preparation. Alternatively, shotgun glycomics approaches have been developed to improve the throughput of glycoprofiling.[5–7]

Mass spectrometry imaging (MSI) is widely used for mapping the spatial distributions of molecules in biological tissues in a label-free fashion.[8–12] Both the experimental implementation and applications of MSI techniques have been extensively reviewed.[9,10,13–17] Imaging of N-linked glycans has been mainly performed using matrix-assisted laser desorption/ionization (MALDI).[18,19] In these experiments, tissues are sectioned and N-linked glycans are enzymatically cleaved from glycoproteins by applying peptide N-glycosidase F (PNGase F) to the tissue.[20] Due to the low ionization yields in negative mode, MALDI MSI of N-linked glycans is commonly performed in positive ionization mode.[21] Meanwhile, on-tissue chemical derivatization is used to stabilize negatively charged species, such as sialylated N-linked glycans, improving the sensitivity of MALDI MSI experiments.[22–24] Recently, MALDI-2 MSI has been used to enhance the ionization of glycans in negative mode, providing access to additional N-linked glycans that cannot be detected using traditional MALDI MSI experiments.[25] This approach also enabled on-tissue MS/MS for the structural characterization of N-linked glycans. Alternatively, ambient ionization techniques are sensitive to analyzing N-linked glycans in both positive and negative ionization mode without the need to stabilize labile sialic acid residues that are known to dissociate in MALDI MSI.[26,27] An ambient electrospray (ESI)-like ionization technique, infrared matrix-assisted laser desorption electrospray ionization (IR-MALDESI), has been used for imaging of N-linked glycans.[28] IR-MALDESI enabled the ionization and detection of labile sialylated N-linked glycans in negative ion mode without the need for chemical derivatization.

In this study, we examine for the first time the potential of an ambient ionization technique based on localized liquid extraction for imaging of N-linked glycans. This class of ionization technique[10,13–15,17,29–31] includes desorption electrospray ionization (DESI)[32], nanospray desorption electrospray ionization (nano-DESI)[17,33], liquid microjunction surface sampling probe[34], liquid extraction surface analysis[35], scanning probe electrospray ionization[36], and single probe[37]. Liquid extraction-based approaches provide the advantage of direct analysis of tissue sections using solvent composition tailored to improve extraction of analytes from the sample[15,17,38,39], enhance ionization efficiency[40,41], and enable online chemical derivatization[42]. Nano-DESI uses localized

liquid extraction followed by electrospray ionization for quantitative mapping of different classes of biomolecules in biological tissue samples with a spatial resolution down to 10 μm.[43] Previous applications of nano-DESI have established its versatility for imaging of metabolites, lipids, and proteins in complex biological tissues.[44–46]

Herein, we demonstrate the potential of nano-DESI MSI to imaging of N-linked glycans in biological tissues both in positive and negative ionization modes without chemical derivatization. To demonstrate the capabilities of the technique, we selected formalin-fixed paraffin-embedded (FFPE) human hepatocellular carcinoma (HCC) and human prostate tissues due to the high abundance of N-linked glycans in these tissues and their biological significance. The tissue samples were prepared using an established method for the enzymatic cleavage of N-linked glycans before the analysis by nano-DESI MSI. We use both positive and negative ion modes to demonstrate the capabilities of nano-DESI MSI for imaging N-linked glycans. On-tissue tandem mass spectrometry (MS/MS) experiments have been used for glycan identification. We have also successfully imaged N-linked glycans in histology-stained tissue sections, which is advantageous to attributing features in ion images to cell types and anatomical structures in tissues. This proof-of-concept study expanding the capabilities of nano-DESI MSI to imaging of N-linked glycans in biological tissues.

Experimental and Methods

Chemicals and Solvent Preparation

Maltoheptaose was purchased from Cayman Chemical (Ann Arbor, MI). $Hex_1HexNAc_2$, Omnisolv LC-MS grade water, acetonitrile (ACN), and methanol (MeOH) were purchased from MilliporeSigma (Burlington, MA). Solutions containing 2 μM $Hex_1HexNAc_2$ were used for optimizing solvent composition for the analysis of N-linked glycans using nano-DESI. We used 7:3 MeOH:H_2O (v/v) containing 5 μM maltoheptaose as a working solvent for nano-DESI MSI experiments.

Tissue Preparation

The prostate cancer and HCC tissues used in this study were purchased from the Hollings Cancer Center Biorepository & Tissue Analysis Core. Use for the study was approved as exemption 4 status by the Medical University of South Carolina Institution Review Board. The FFPE human tissue samples were prepared for nano-DESI MSI using established methods briefly described below.[47]

Dewaxing/Delipidation

The FFPE human tissue sections were heated at 60°C for 1 hr to melt the paraffin residue around the tissue sections. After heating the FFPE tissue sections were cooled to room temperature. The tissue sections underwent a series of eight washes in Coplin jars to eliminate salts, metabolites, and lipids. The washes were performed using histology-grade xylenes (x2, 3 min), 100% ethanol

(x2, 1 min), 95% ethanol (1 min), 70% ethanol (1min), and LC-MS grade water (x2, 3 min each). The washed tissue sections were placed in a vacuum desiccator for 5-min.

Antigen Retrieval

A vegetable steamer (Rival, Kansas City, Missouri, USA) was filled with distilled water and heated for antigen retrieval. The tissue sections were placed in the steamer for 30 min inside a five-slide mailer with a side opening, which contained 10mL of 10 mM citraconic acid buffer (pH 3, Sigma-Aldrich, St. Louis, MO, USA). Next, the slide mailer was removed from the steamer and immersed in cool water for 5 min until tissue sections reached room temperature. Tissue sections were cooled by removing half of the buffer, replacing it with LC-MS grade water, and incubating for 5 min. This process was repeated 2 times. Subsequently, the tissue sections were rinsed with LC-MS grade water and placed in a vacuum desiccator for 5 min.

Enzymatic Digestion of N-Linked Glycans

PNGase F PRIME-LY (Bulldog Bio, Portsmouth, NH, USA) was uniformly applied to the tissues using a TM-Sprayer (HT-X Technologies, Carrboro, NC, USA) at 25µL/min, 1200 mm/min velocity, 3 mm spacing, and 15 passes in a crisscross pattern, nozzle heated to 45°C, and nitrogen gas pressure was 10 psi. The tissue sections were then incubated at 37°C for 2 hrs in preheated humidity chambers to enzymatically cleave N-linked glycans.

Mass Spectrometry

Electrospray ionization MS (ESI-MS) experiments were performed on a LTQ-XL linear quadrupole ion trap mass spectrometer (Thermo Fisher Scientific, Waltham, MA) using solvent compositions of 1:1 MeOH:H_2O, 8:2 MeOH:H_2O, 1:1 9:1 MeOH:H_2O, and 6.5:3.5 ACN:H_2O. Additional ESI-MS experiments were performed on a Q-Exactive HF-X Orbitrap mass spectrometer (Thermo Fisher Scientific, Waltham, MA) using solvent compositions of 7:3 MeOH:H_2O and 8:2 MeOH:H_2O. In both ESI-MS experiments, the solvent was infused using a syringe pump at 0.5 µL/min. ESI-MS was performed in positive ionization mode achieved by applying a 5 kV potential to the syringe needle. The heated capillary inlet was at 300 °C. Mass spectra were acquired with a mass resolution of ($m/\Delta m$) 7,500 at m/z 200 on the LTQ-XL and with a mass resolution of ($m/\Delta m$) of 60,000 at m/z 200 on the Q-Exactive HF-X.

Nano-DESI analysis

Experiments were performed using a custom designed nano-DESI source on a Q-Exactive HF-X Orbitrap mass spectrometer described in detail in our previous publications.[48,49] Briefly, the nano-DESI probe is composed of two fused silica capillaries (OD 150 µm x ID 50 µm) that form a liquid bridge on a sample surface. The primary capillary delivers the extraction solvent to the sample and the nanospray capillary transfers the extracted analytes to a mass spectrometry inlet, where they undergo electrospray-like ionization. A third fused silica capillary (200 µm ID, 790 µm OD) pulled to ~20 µm OD using a P-2000 puller (Sutter instrument, Novato, CA) serves as a shear force probe. The shear force probe controls the distance between the sample and nano-DESI probe.[48,50] High-

resolution micromanipulators (5, XYZ500TIM, Quater Research and Development, Bend, OR) are used to position all capillaries in front of the mass spectrometer inlet. Two Dino-Lite microscope cameras assist in the placement of both the nano-DESI and shear force probes.

For nano-DESI MSI experiments, the working solvent is delivered at a rate of 0.5 µL/min by the syringe pump. Data acquisition was performed in both positive and negative ionization modes. Ionization was achieved by applying (±) 5.0 kV potential to the syringe needle for both ionization modes. The heated capillary inlet was held at 300°C. Mass spectra were acquired with a mass resolution of ($m/\Delta m$) of 60,000 at *m/z* 200. Imaging data were acquired in lines at a scan rate of 40 µm/s and a step between the lines of 150 µM. Data-dependent MS/MS spectra were acquired directly from the tissue using higher-energy collision-induced (HCD) with a mass isolation window of 0.5 *m/z* and HCD energy of 30 arbitrary units specific to the instrument.

For imaging of prostate cancer tissues, we used *m/z* ranges of 200-3,000 and 300-3,000 in positive and negative ion mode, respectively. For imaging of HCC tissues, multiple selected ion monitoring (SIM) scans were used to preconcentrate low-abundant ions within a narrow *m/z* window. The instrument method was designed to acquire mass spectra from each *m/z* window in sequence while the sample is scanned under the nano-DESI probe. As a result, each pixel of the image contains information from multiple SIM windows. A data acquisition rate of 1 Hz was used for SIM, while7 Hz was used for full MS mode. Alternating between line scans of both full MS mode and SIM methods were performed on the same tissue section to ensure accurate comparison between the results obtained using these acquisition modes. Lines acquired with only full MS scans in positive ion mode used an *m/z* range of 200-3,000. Lines acquired with SIM mode and full MS scans are listed in Table 1. In both modes, the automatic gain control (AGC) was set to a target of $1x10^6$. This value was selected to ensure an equal number of charges were analyzed in both full MS and SIM modes for an accurate comparison. The maximum IT time was set to 500 ms, but typically remained below 200 ms.

Table 1. List of scan windows used for imaging HCC tissues in positive ion mode.

Scan Type	*m/z* window
Full ms	300-2500
SIM	820-870
SIM	900-950
SIM	1400-1450
Full ms	1500-1600
SIM	1650-1700
SIM	1730-1780
SIM	1800-1850
SIM	2095-2145

Data Analysis

Each line scan was acquired as an individual file (.RAW file format) using Xcalibur software (Thermo Electron, Bremen, Germany). Data processing was performed using a Python code developed by our group (https://github.com/hanghu1024/RAW-MSI-generator). Ion images were constructed by plotting ion abundances of targeted *m/z* features within the mass tolerance window of ±10 ppm in each mass spectrum (pixel) as a function of the location on the tissue normalized to the total ion count (TIC). To accurately reconstruct ion images for data acquired using SIM scans, the pixels in the scan direction were aligned based on the experiment time stamp (scan time) as previously described by our group.[51] Next, GlycoHunter was used to create an initial peak list from the experimental nano-DESI MSI data. Singly and doubly charged ions were identified by searching isotopic peaks separated by 1.0 (z=1) and 0.5 (z=2) *m/z* in the data with a ±10 ppm *m/z* tolerance and a minimum abundance threshold of 1000 ions/scan.[52] Candidate assignments were searched with GlycoMod[53], a theoretical glycan database, where each identification was made with a corresponding match to GlyConnect[54], an experimentally curated glycomic database. The criteria for identification using Glyconnect were as follows: a ±10 ppm *m/z* tolerance, presence of $Hex_3HexNAc_2$, and exclusion of pentose, KDN, or HexA monosaccharides. Further identification of putative structures was made with GlycoWorkbench and in silico fragmentation was used to match with the experimental MS/MS data.[55]

Results and Discussion

In this study, we use nano-DESI MSI to spatially map the distributions of N-linked glycans in two different biological tissue samples: FFPE human HCC and prostate tissue. The experimental workflow includes standard sample preparation steps required for imaging of N-linked glycans. For FFPE tissues sections, tissue washes in xylene, ethanol, and water are carried out to remove paraffin residue, salts, metabolites, and lipids to expose proteins in the sample. Antigen retrieval is performed to remove protein cross-linking thereby providing the enzyme access to the glycosylation sites. Next, PNGase F is pneumatically sprayed over the tissue sections, followed by digestion at 37°C in a humidity chamber. The enzymatically cleaved N-linked glycans are then analyzed by nano-DESI MSI.

We optimized the solvent composition by measuring the signal of the $[M+Na]^+$ ion of an N-glycan standard, $Hex_1HexNAc_2$, produced by electrospray ionization of a 2 µM $Hex_1HexNAc_2$ solution in five different solvents: 1:1 MeOH:H_2O, 7:3 MeOH:H_2O, 8:2 MeOH:H_2O, 9:1 MeOH:H_2O, and 6.5:3.5 ACN:H_2O. The 9:1 MeOH:H_2O mixture is typically used in nano-DESI MSI of lipids and metabolites. Meanwhile, the 6.5:3.5 ACN:H_2O mixture was used in the first IR-MALDESI analysis of N-linked glycans.[28] Because N-linked glycans are hydrophilic molecules, they are expected to be better extracted into a solvent containing a higher percentage of H_2O. Indeed, we observed the highest signal of $Hex_1HexNAc_2$ in 7:3 MeOH:H_2O and used this solvent composition in nano-DESI MSI experiments.

We performed imaging of N-linked glycans by nano-DESI in both positive and negative ionization modes. N-linked glycans were detected as both singly and doubly sodiated species in positive mode and as deprotonated species and chloride adducts in negative mode. A total of 38 native N-

linked glycans including high-mannose, hybrid fucosylated, and sialylated species were observed by nano-DESI MSI between both HCC and prostate tissue sections. A complete list of the observed species is provided in Tables S1 and S2. Among the observed N-linked glycans, 37% were fucosylated and 24% were sialylated species containing at least one sialic acid residue.

Nano-DESI MSI of Hepatocellular Carcinoma Tissue Sections

We selected HCC tissue as a model system that has been previously studied using MALDI MSI.[56–58] HCC is the most common form of liver cancer accounting for ~90% of all liver cancer cases and ranking as the third leading cause of cancer-related deaths in 2020.[59,60] N-linked glycan distribution has been identified as potential biomarkers of HCC, making this tissue an important target for understanding glycosylation using MSI.[56–58] We used nano-DESI MSI to distinguish regions of interest based on the localization of N-linked glycans in HCC tissue. An image of the H&E-stained tissue shown in Fig. 1A displays distinct regions, including hepatocytes, stroma/extracellular matrix, and tumors highlighted in Fig. 1B with green, red, and blue, respectively. An averaged mass spectrum obtained from a line scan across the HCC tissue is shown in Fig.1C. Doubly charged sodiated species, marked by pink dashed lines in Fig. 1C, constitute the majority of N-linked glycans observed in the mass spectrum. Sialylated N-linked glycans, marked by purple dashed lines in Fig. 1C, are observed as $[M+3Na-H]^{2+}$ ions due to neutral exchange of an acidic proton on the sialic acid with a sodium ion. Several N-linked glycans are observed as both singly and doubly charged sodiated species. Singly charged N-linked glycans above *m/z* 1,400 appear in low abundance in the full mass spectrum, which limits the sensitivity of nano-DESI MSI performed in the broadband detection mode.

To increase the sensitivity of nano-DESI MSI experiments, we used SIM mode. This method utilizes several narrow *m/z* windows to increase the signals of low-abundance species.[61] Consequently, each pixel of the image contains information from multiple SIM windows. In this study, we used SIM windows listed in Table 1 that include a majority of the observed N-linked glycans. Fig. 2 provides a comparison of the signal observed for $Hex_5HexNAc_4$ at *m/z* 1663.5837 in full MS (Fig. 2A) and SIM mode (Fig. 2B). An optical image of the tissue section is shown in Fig. 2C and the corresponding ion images obtained in full MS and SIM modes are shown in Figs. 2D and 2E, respectively.

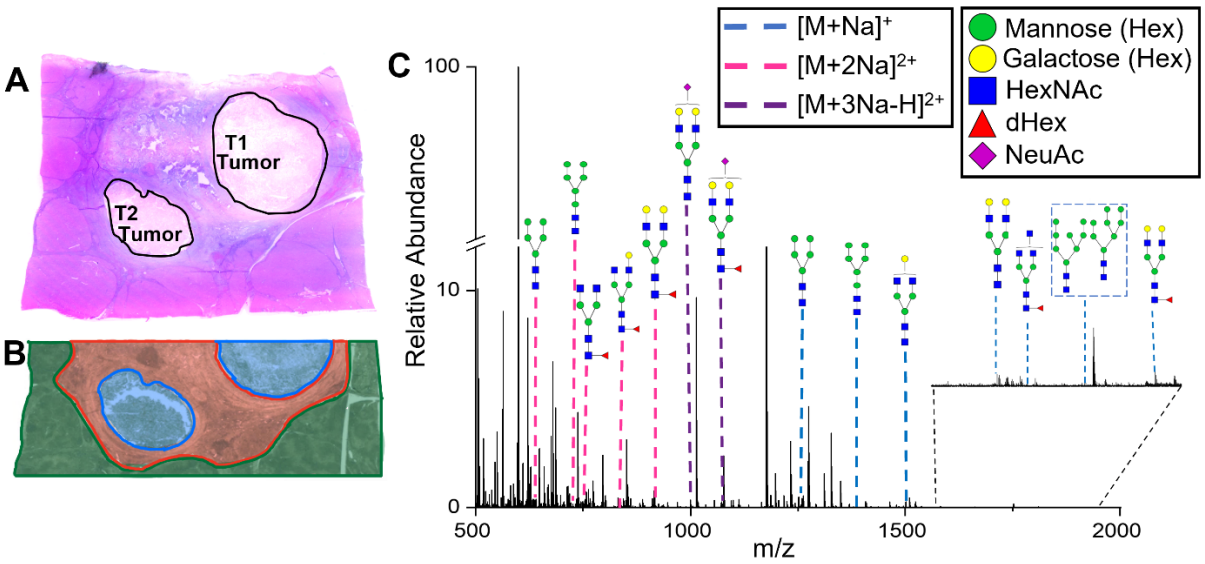

Figure 1. (A) Optical image of the H&E stained FFPE hepatocellular carcinoma tissue section and (B) optical image with regions of interest identified to be hepatocytes (green), stroma and extracellular matrix (red), and HCC (blue). (C) N-linked glycan profile obtained from a line scan across the HCC tissue section. The internal standard is seen as the major peaks at *m/z* 1175.3696 as $[M+Na]^+$, *m/z* 1013.3193 as $[M-Hex+Na]^+$, and *m/z* 599.1794 as $[M+2Na]^{2+}$ in the spectra.

Averaged mass spectra acquired in full MS and SIM modes are shown in Figs. 2A and 2B, respectively. In full MS mode, the signal of the $[M+Na]^+$ ion of $Hex_5HexNAc_4$ at *m/z* 1663.5837 of 1.1 $x10^2$ is close to the noise level. In SIM mode, the signal increases to $1.8x10^3$ as shown in Fig. 2B. Ion images obtained in both full MS (Fig. 2D) and SIM mode (Fig. 2E) demonstrate the effect of the 16-fold increase in ion signal on the quality of nano-DESI MSI data. In particular, the distribution of $Hex_5HexNAc_4$ cannot be determined using full MS acquisition mode. In contrast, SIM mode reveals the localization of $Hex_5HexNAc_4$ to the tumor regions in the HCC tissue. Additionally, as depicted in Fig. S1, we observe an increase in signal-to-noise for doubly sodiated species in SIM mode compared to full MS mode, indicating the improved ion image quality obtained in SIM mode. We conclude that SIM mode enhances the sensitivity and quality of nano-DESI MSI data, enabling the localization of N-linked glycans in the HCC tissue.

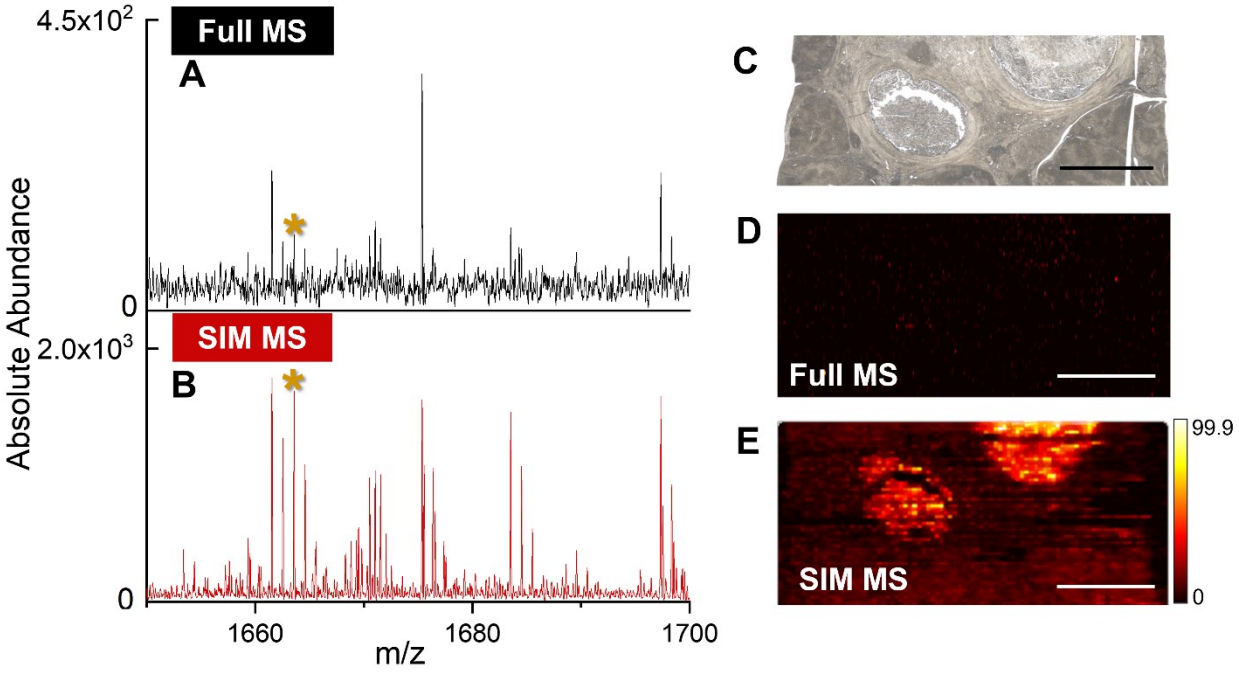

Figure 2. Mass spectra averaged over adjacent line scans acquired in (A) full MS and (B) SIM modes to indicate ion signal of $Hex_5HexNAc_4$ (*m/z* 1663.5837; $[M+Na]^+$) marked by a yellow asterisk. (C) Optical image of the HCC tissue section and the corresponding ion images of $Hex_5HexNAc_4$ acquired in (D) full and (E) SIM MS modes. Scale bar is 5 mm. The ion images are normalized to TIC and the corresponding normalized ion abundance scale is shown at the 99.9 percentile.

To examine whether nano-DESI MSI is compatible with histopathological imaging, we performed imaging of N-linked glycans in H&E-stained tissue sections. In these experiments, we compared the distribution of N-linked glycans in two similar HCC tissue sections: one prepared with only the application of PNGase F and a consecutive one subjected to H&E staining followed by PNGase F application shown in Fig. 3A and 3B, respectively. Optical images of the two sections and the corresponding TIC-normalized ion images of N-linked glycans are shown in Fig. 3. There is a good correspondence between both the abundance and localization of the N-linked glycans in the two HCC tissue sections. This result demonstrates that the current multiplexed imaging protocol for MALDI MSI analysis is also compatible with nano-DESI MSI experiments.[62] Comparable localizations of N-linked glycans are observed in the regions of interest in the HCC tissue including hepatocytes, stroma and extracellular matrix, and HCC. These regions were described earlier and are highlighted in Fig. 1B. For example, $Hex_5HexNAc_4$ at *m/z* 843.2872 observed as a $[M+2Na]^{2+}$ ion is present in the tumor regions with increased ion signal observed in tumor 1. Another doubly sodiated species, $Hex_5dHex_1HexNAc_4$ at *m/z* 916.3163 is localized to both the tumor and stroma regions of the HCC tissue. Meanwhile the singly sodiated species, $Hex_3HexNAc_2$ at *m/z* 933.3197 is present in both the tumor and hepatocyte regions and $Hex_8HexNAc_2$ at *m/z* 1743.5909 is mainly present in the hepatocyte region. These observations are consistent with a previous study, in which

MALDI MSI was used to examine the distributions of N-linked glycans in HCC tissue.[63] In that study, high mannose glycans such as $Hex_5HexNAc_2$ were found to be elevated in the tumor tissue while fucosylated complex biantennary glycans such as $Hex_5dHex_1HexNAc_4$ were elevated in the stroma and extracellular matrix region.[63] The multiplexed imaging of tissues using nano-DESI MSI and H&E staining is important for placing the molecular information obtained from nano-DESI MSI experiments into the context of tissue histopathology.

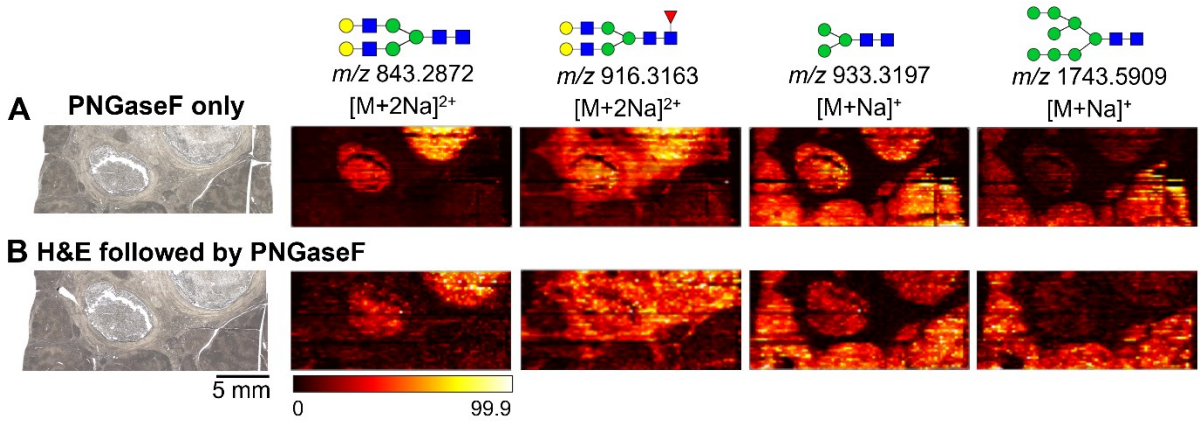

Figure 3. Optical images of HCC tissue sections with the (A) application of PNGase F only and (B) H&E followed by PNGase F application in positive ion mode. TIC-normalized nano-DESI images of $Hex_5HexNAc_4$ (*m/z* 843.2872; $[M+2Na]^{2+}$), $Hex_5dHex_1HexNAc_4$ (*m/z* 916.3163; $[M+2Na]^{2+}$), $Hex_3HexNAc_2$ (*m/z* 933.3197; $[M+Na]^{+}$), $Hex_8HexNAc_2$ (*m/z* 1743.5909; $[M+Na]^{+}$). Scale bar is 5 mm. The normalized ion abundance scale is shown at the 99.9 percentile.

Prostate Tissue Imaging

We have also conducted imaging of N-linked glycans in FFPE human prostate tissue sections using nano-DESI in both positive and negative ionization modes. Fig. 4 shows the corresponding optical and ion images of N-linked glycans acquired in positive and negative modes. Optical images of an H&E stained prostate tissue section and two adjacent prostate tissue sections used for imaging in positive and negative mode are shown in Figs. 4A-C, respectively. Ion images of the N-linked glycans observed in positive mode are shown in Fig. 4D. The most abundant N-linked glycans in positive mode include $[M+2Na]^{2+}$ ions of $Hex_5HexNAc_4$ at *m/z* 843.2878 and $Hex_5dHex_1HexNAc_4$ at *m/z* 916.3165, and an $[M+3Na-H]^{2+}$ ion of a sialylated glycan, $Hex_5dHex_1HexNAc_4NeuAc_1$ at *m/z* 1072.8572 and are localized to the stroma regions. The high mannose N-linked glycan, $Hex_6HexNAc_2$ at *m/z* 721.2344 observed as a $[M+2Na]^{2+}$ species is localized to the lumen region. These observations are consistent with previous studies mapping N-linked glycan distributions with MALDI MSI, in which core-fucosylated N-linked glycans such as $Hex_5HexNAc_4NeuAc_1$ and $Hex_5dHex_1HexNAc_4NeuAc_1$ are observed in the stroma region and high-mannose N-linked glycans such as $Hex_6HexNAc_2$ and $Hex_7HexNAc_6$ are observed in the lumen regions.[64,65]

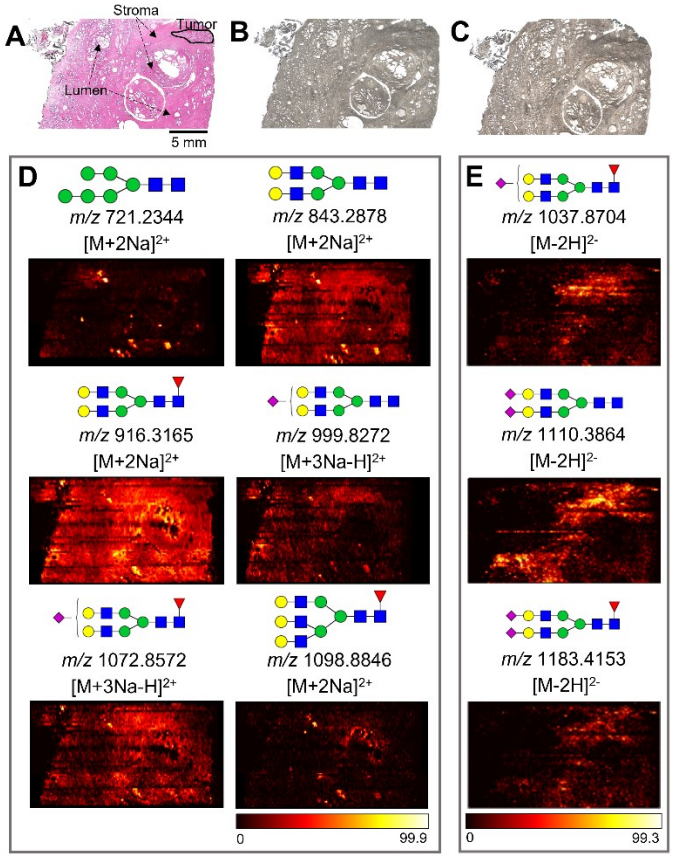

Figure 4. Optical images of (A) H&E-stained prostate cancer tissue with the tumor region outlined in black, (B) FFPE prostate cancer tissue for positive ion mode, and (C) FFPE prostate tissue for negative ion mode used in nano-DESI MSI. (D) Ion images of $Hex_6HexNAc_2$ (*m/z* 721.2344; $[M+2Na]^{2+}$), $Hex_5HexNAc_4$ (*m/z* 843.2878; $[M+2Na]^{2+}$), $Hex_5dHex_1HexNAc_4$ (*m/z* 916.3165; $[M+2Na]^{2+}$), $Hex_5HexNAc_4NeuAc_1$ (*m/z* 999.8272; $[M+3Na-H]^{2+}$), $Hex_5dHex_1HexNAc_4NeuAc_1$ (*m/z* 1072.8572; $[M+3Na-H]^{2+}$), and $Hex_6dHex_1HexNAc_5$ (*m/z* 1098.8846; $[M+2Na]^{2+}$) obtained in positive ion mode. (E) Ion images of $Hex_5dHex_1HexNAc_4NeuAc1$ (*m/z* 1037.8704; $[M-2H]^{2-}$), $Hex_5HexNAc_4NeuAc_2$ (*m/z* 1110.3864; $[M-2H]^{2-}$), $Hex_5dHex_1HexNAc_4NeuAc_2$ (*m/z* 1183.4153; $[M-2H]^{2-}$) obtained in negative ion mode. Scale bar is 5 mm. All ion images are normalized to TIC and the corresponding normalized ion abundance scale is shown at the 99.9 percentile for positive ion mode and 99.3 percentile for negative ion mode.

Ion images obtained in negative mode (Fig.4E) highlight the localization of sialylated N-linked glycans. Sialylated N-linked glycans were readily observed in negative ion mode as intact species. Furthermore, five N-glycans observed exclusively in negative ion mode include, $Hex_4dHex_1HexNAc_5NeuAc_1$, $Hex_5dHex_1HexNAc_4$, $Hex_5dHex_1HexNAc4NeuAc_2$, and $Hex_6HexNAc_5NeuAc_3$. Their efficient ionization in nano-DESI is attributed to the presence of a negative charge on the carboxylic residue of the sialic acid on the N-linked glycans. This indicates that nano-DESI is a 'soft' ionization technique that preserves labile sialic acid species without requiring chemical derivatization. Sialylated N-linked glycans have been previously detected directly from tissues using IR-MALDESI experiments in negative ionization mode.[28] Similar to

MALDI-MSI, we also observe a minor amount of in-source fragmentation. We evaluate the neutral loss of a hexose for the singly and doubly sodiated species of the standard, maltoheptaose, observed in the mass spectra shown in Fig. S2. We estimate the extent of in-source fragmentation to be ~10% for $[M+Na]^+$ ions and <5% for $[M+2Na]^{2+}$ ions. Based on the results of nano-DESI MSI, this minor in-source fragmentation does not have a measurable effect. Overall, the nano-DESI MSI experiments revealed that sialylated N-linked glycans constituted 66% of native N-linked glycans observed in negative ion mode as compared to only 17% in positive mode. We observed 34 N-linked glycans in HCC and 38 species in prostate tissue samples using nano-DESI MSI. This result is comparable to MALDI MSI study by Powers et al., in which 33 species were detected in HCC tissue.[63] A more recent MALDI MSI by DelaCourt et al. reported the detection of 51 N-linked glycans in HCC tissue.[58] Meanwhile, a significantly larger number of N-linked glycans have been observed in prostate tissue using IR-MALDESI (53 species) and MALDI MSI (73 species).[28,64] Although the results obtained using nano-DESI MSI are fairly close to what has been reported using more established MSI modalities for imaging of N-linked glycans, further optimization of tissue preparation and solvent composition is required to improve the performance of this technique for glycan imaging. Nevertheless, this first proof-of-concept study demonstrates that nano-DESI MSI is well-suited for studying the localization of N-glycans in tissues, which expands the range of applications of this imaging technique.

Sequence Elucidation by on-tissue MS/MS of N-linked Glycans

Tandem mass spectrometry (MS/MS) was performed to elucidate the structures of the observed N-linked glycans. Fragment ions were assigned according to the Domon and Costello nomenclature.[66] Briefly, glycosidic fragments containing the reducing end of a N-linked glycan are designated as X, Y, and Z. Glycosidic fragments containing the non-reducing end of N-linked glycans are designated as A, B, and C. The MS/MS of $Hex_5dHex_1HexNAc_4$ of the singly and doubly sodiated adducts are shown in Fig. 5. The MS/MS spectrum of different adducts provide complementary information about the glycan sequence.

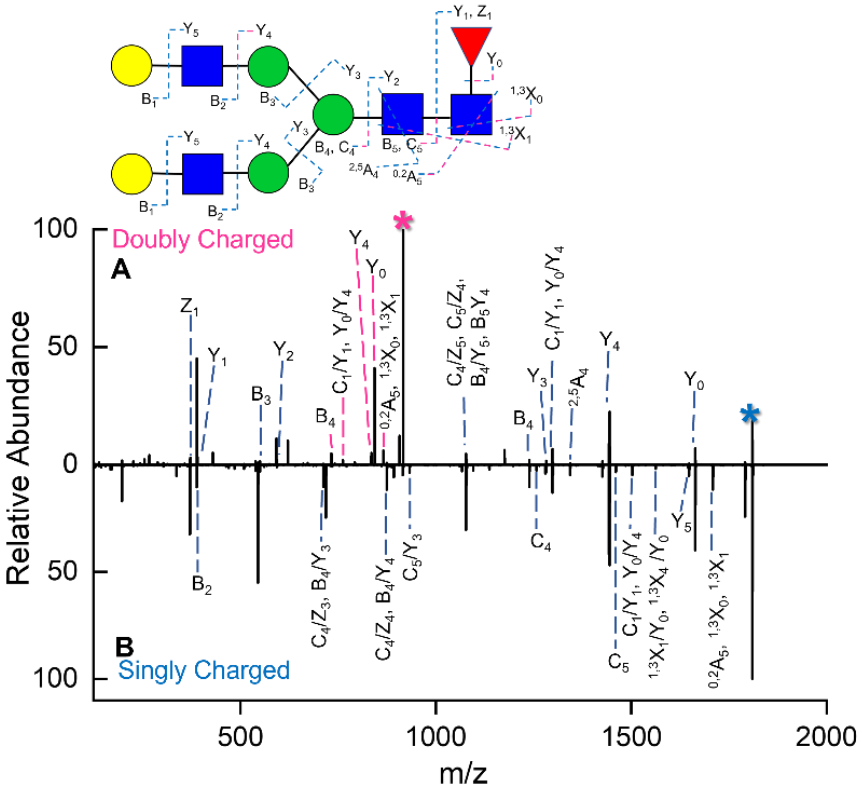

Figure 5. Fragmentation spectra of $Hex_5dHex_1HexNAc_4$ of adducts in the form of (B) $[M+2Na]^{2+}$ at *m/z* 916.3165 (pink asterisk) and (C) $[M+Na]^{+}$ at *m/z* 1809.6456 (blue asterisk). Singly charged cleavages are denoted with blue dashed line. Doubly charged cleavages are denoted with a pink dashed line. Cross-ring cleavages, A and X, include superscript numbers indicating the cleaved linkages in the sugar ring. The subscript number indicates the location of the cleavage. Labels with two cleavage sites are linked with a slash to indicate internal fragment ions generated from cleavage at both locations.

Loss of a sodium ion is one of the major dissociation pathways observed for the $[M+2Na]^{2+}$ precursor (Fig. 5A), which is consistent with previous studies focused on CID of doubly sodiated glycans.[67] Meanwhile, the MS/MS spectrum of $[M+Na]^{+}$ (Fig. 5B) is dominated by glycosidic cleavages resulting in formation of abundant B and Y ions. Glycosidic bond cleavages make up ~70% of the observed fragment ions of $[M+2Na]^{2+}$ and ~ 60% of the observed fragment ions of $[M+Na]^{+}$. MS/MS spectra of both adducts contain the Y_0 fragment, which corresponds to the loss of the core fucose. The presence of a core fucose is confirmed by fragments containing the non-reducing end of the N-linked glycan such as B_4 and B_5 ions that do not include fucose. Several internal fragments produced by a combination of two bond cleavages are observed in both MS/MS spectra in comparable abundance. Other fragment ions including Z_1, B_2, B_4, and Y_4, appear in both spectra, but in differing abundance. However, Y_1 and Y_2 fragments corresponding to glycosidic cleavages appear only in the MS/MS spectrum of $[M+2Na]^{2+}$. Meanwhile, C_4, C_5, and Y_5 fragments appear only in the MS/MS spectrum of $[M+Na]^{+}$. Collectively, HCD of both adducts contain fragment ions corresponding to glycosidic cleavages at each sugar-sugar bond. The differences in the observed fragmentation of the $[M+2Na]^{2+}$ and $[M+Na]^{+}$ precursors provide

additional structural information necessary for identifying the sugar sequence of $Hex_5dHex_1HexNAc_4$. Of the N-linked glycans assignments observed in positive mode in this study, nine were confirmed by examining glycosidic cleavages observed in the MS/MS data shown in Fig. S3.

Conclusion

We have developed a method to spatially map N-linked glycans in biological tissues using nano-DESI MSI. The approach is compatible with H&E staining, which is advantageous for multiplexed imaging of tissue sections. Nano-DESI is well-suited for analyzing N-linked glycans in heterogenous tissues in both positive and negative ionization modes, as demonstrated by observing 38 N-linked glycans in this study. The formation of multiple adducts favored in nano-DESI MSI enhances the structural information obtained using on-tissue MS/MS of N-linked glycans. The collective fragmentation patterns observed in the MS/MS spectra enable elucidation of the glycan sequence. This proof-of-concept study provides a foundation for future multiplexed imaging of N-linked glycans and peptides. Further research is required to optimize the extraction solvent and instrumentation to improve the detection of native N-linked glycans by nano-DESI. Our results showcase the potential of nano-DESI MSI to spatially characterize N-linked glycans in biological tissues.

Supporting Information:

Lists of N-Linked glycans detected in positive and negative ion mode (Tables S1 and S2); comparison of full MS and SIM modes for doubly sodiated species on HCC tissues (Figures S1); mass spectrum and ion images evaluating the in-source fragmentation of maltoheptaose (Figures S2); MS/MS spectra of N-linked glycans (Figures S3). (PDF)

Acknowledgements

The authors gratefully acknowledge the financial support from the National Science Foundation (NSF-2108729, JL) and Center for Bioanalytical Metrology, an NSF Industry-University Cooperative Research Center (Grant IIP-1916691). Supported in part by the Hollings Cancer Center Biorepository & Tissue Analysis Shared Resource, Hollings Cancer Center, Medical University of South Carolina (P30 CA138313). PMA and RRD acknowledge support by NIH/NCI U01242096, NIH/NCI R21CA263464, NIH/NCI U01CA242096 and NIH/NCI R33CA267226. We also thank Dr. Michael Easterling from Bruker Daltonics for helpful discussions.

References

(1) Hart, G. W.; Copeland, R. J. Glycomics Hits the Big Time. Cell 2010, 143 (5), 672. https://doi.org/10.1016/J.CELL.2010.11.008.

(2) Varki, A. Biological Roles of Glycans. Glycobiology 2017, 27 (1), 3–49. https://doi.org/10.1093/glycob/cww086.

(3) Ohtsubo, K.; Marth, J. D. Glycosylation in Cellular Mechanisms of Health and Disease. Cell 2006, 126 (5), 855–867. https://doi.org/10.1016/J.CELL.2006.08.019.

(4) Ruhaak, L. R.; Xu, G.; Li, Q.; Goonatilleke, E.; Lebrilla, C. B. Mass Spectrometry Approaches to Glycomic and Glycoproteomic Analyses. Chem Rev 2018, 118 (17), 7886–7930. https://doi.org/10.1021/ACS.CHEMREV.7B00732.

(5) de Haan, N.; Pučić-Baković, M.; Novokmet, M.; Falck, D.; Lageveen-Kammeijer, G.; Razdorov, G.; Vučković, F.; Trbojević-Akmačić, I.; Gornik, O.; Hanić, M.; Wuhrer, M.; Lauc, G.; Guttman, A.; Cummings, R.; Mora, S.; Rombouts, Y.; Mehta, A. Developments and Perspectives in High-Throughput Protein Glycomics: Enabling the Analysis of Thousands of Samples. Glycobiology 2022, 32 (8), 651–663. https://doi.org/10.1093/GLYCOB/CWAC026.

(6) Cummings, R. D.; Pierce, J. M. The Challenge and Promise of Glycomics. Chem Biol 2014, 21 (1), 1–15. https://doi.org/10.1016/J.CHEMBIOL.2013.12.010.

(7) Trbojević-Akmačić, I.; Lageveen-Kammeijer, G. S. M.; Heijs, B.; Petrović, T.; Deriš, H.; Wuhrer, M.; Lauc, G. High-Throughput Glycomic Methods. Chem Rev 2022, 122 (20), 15865–15913. https://doi.org/10.1021/ACS.CHEMREV.1C01031.

(8) Mcdonnell, L. A.; Heeren, R. M. A. Imaging Mass Spectrometry. Mass Spectrom Rev 2007, 26 (4), 606–643. https://doi.org/10.1002/mas.20124.

(9) Gode, D.; Volmer, D. A. Lipid Imaging by Mass Spectrometry-a Review. Analyst 2013, 138 (5), 1289–1315. https://doi.org/10.1039/c2an36337b.

(10) Norris, J. L.; Caprioli, R. M. Imaging Mass Spectrometry: A New Tool for Pathology in a Molecular Age. Proteomics Clin Appl 2013, 7 (11–12), 733–738. https://doi.org/10.1002/prca.201300055.

(11) Stoeckli, M.; Chaurand, P.; Hallahan, D. E.; Caprioli, R. M. Imaging Mass Spectrometry: A New Technology for the Analysis of Protein Expression in Mammalian Tissues. Nature Medicine 2001 7:4 2001, 7 (4), 493–496. https://doi.org/10.1038/86573.

(12) Buchberger, A. R.; DeLaney, K.; Johnson, J.; Li, L. Mass Spectrometry Imaging: A Review of Emerging Advancements and Future Insights. Anal Chem 2018, 90 (1), 240. https://doi.org/10.1021/ACS.ANALCHEM.7B04733.

(13) Xiao, Y.; Deng, J.; Yao, Y.; Fang, L.; Yang, Y.; Luan, T. Recent Advances of Ambient Mass Spectrometry Imaging for Biological Tissues: A Review. Anal Chim Acta 2020, 1117, 74–88. https://doi.org/10.1016/j.aca.2020.01.052.

(14) Perez, C. J.; Bagga, A. K.; Prova, S. S.; Yousefi Taemeh, M.; Ifa, D. R. Review and Perspectives on the Applications of Mass Spectrometry Imaging under Ambient Conditions. Rapid Communications in Mass Spectrometry 2019, 33 (S3), 27–53. https://doi.org/10.1002/rcm.8145.

(15) Wu, C.; Dill, A. L.; Eberlin, L. S.; Cooks, R. G.; Ifa, D. R. Mass Spectrometry Imaging under Ambient Conditions. Mass Spectrom Rev 2013, 32 (3), 218–243. https://doi.org/10.1002/mas.21360.

(16) Zemski Berry, K. A.; Hankin, J. A.; Barkley, R. M.; Spraggins, J. M.; Caprioli, R. M.; Murphy, R. C. MALDI Imaging of Lipid Biochemistry in Tissues by Mass Spectrometry. Chem Rev 2011, 111 (10), 6491–6512. https://doi.org/10.1021/cr200280p.

(17) Laskin, J.; Lanekoff, I. Ambient Mass Spectrometry Imaging Using Direct Liquid Extraction Techniques. Anal Chem 2016, 88 (1), 52–73. https://doi.org/10.1021/acs.analchem.5b04188.

(18) McDowell, C. T.; Lu, X.; Mehta, A. S.; Angel, P. M.; Drake, R. R. Applications and Continued Evolution of Glycan Imaging Mass Spectrometry. Mass Spectrom Rev 2023, 42 (2), 674. https://doi.org/10.1002/MAS.21725.

(19) Powers, T. W.; Neely, B. A.; Shao, Y.; Tang, H.; Troyer, D. A.; Mehta, A. S.; Haab, B. B.; Drake, R. R. MALDI Imaging Mass Spectrometry Profiling of N-Glycans in Formalin-Fixed Paraffin Embedded Clinical Tissue Blocks and Tissue Microarrays. PLoS One 2014, 9 (9), e106255. https://doi.org/10.1371/JOURNAL.PONE.0106255.

(20) Powers, T. W.; Jones, E. E.; Betesh, L. R.; Romano, P. R.; Gao, P.; Copland, J. A.; Mehta, A. S.; Drake, R. R. Matrix Assisted Laser Desorption Ionization Imaging Mass Spectrometry Workflow for Spatial Profiling Analysis of N-Linked Glycan Expression in Tissues. Anal Chem 2013, 85 (20), 9799–9806. https://doi.org/10.1021/AC402108X.

(21) Harvey, D. J. Structural Determination of N-Linked Glycans by Matrix-Assisted Laser Desorption/Ionization and Electrospray Ionization Mass

Spectrometry. Proteomics 2005, 5 (7), 1774–1786. https://doi.org/10.1002/PMIC.200401248.

(22) Holst, S.; Heijs, B.; De Haan, N.; Van Zeijl, R. J. M.; Briaire-De Bruijn, I. H.; Van Pelt, G. W.; Mehta, A. S.; Angel, P. M.; Mesker, W. E.; Tollenaar, R. A.; Drake, R. R.; Bovée, J. V. M. G.; McDonnell, L. A.; Wuhrer, M. Linkage-Specific in Situ Sialic Acid Derivatization for N-Glycan Mass Spectrometry Imaging of Formalin-Fixed Paraffin-Embedded Tissues. Anal Chem 2016, 88 (11), 5904–5913. https://doi.org/10.1021/acs.analchem.6b00819.

(23) de Haan, N.; Yang, S.; Cipollo, J.; Wuhrer, M. Glycomics Studies Using Sialic Acid Derivatization and Mass Spectrometry. Nature Reviews Chemistry 2020 4:5 2020, 4 (5), 229–242. https://doi.org/10.1038/s41570-020-0174-3.

(24) Lu, X.; McDowell, C. T.; Blaschke, C. R. K.; Liu, L.; Grimsley, G.; Wisniewski, L.; Gao, C. F.; Mehta, A. S.; Haab, B. B.; Angel, P. M.; Drake, R. R. Bioorthogonal Chemical Labeling Probes Targeting Sialic Acid Isomers for N-Glycan MALDI Imaging Mass Spectrometry of Tissues, Cells, and Biofluids. Anal Chem 2023, 95 (19), 7475–7486. https://doi.org/10.1021/ACS.ANALCHEM.2C04882.

(25) Heijs, B.; Potthoff, A.; Soltwisch, J.; Dreisewerd, K. MALDI-2 for the Enhanced Analysis of N-Linked Glycans by Mass Spectrometry Imaging. Anal Chem 2020, 92 (20), 13904–13911. https://doi.org/10.1021/acs.analchem.0c02732.

(26) Pace, C. L.; Muddiman, D. C. Direct Analysis of Native N-Linked Glycans by IR-MALDESI. J Am Soc Mass Spectrom 2020, 31 (8), 1759–1762. https://doi.org/10.1021/JASMS.0C00176.

(27) Zaia, J. Mass Spectrometry and Glycomics. OMICS 2010, 14 (4), 401. https://doi.org/10.1089/OMI.2009.0146.

(28) Pace, C. L.; Angel, P. M.; Drake, R. R.; Muddiman, D. C. Mass Spectrometry Imaging of N-Linked Glycans in a Formalin-Fixed Paraffin-Embedded Human Prostate by Infrared Matrix-Assisted Laser Desorption Electrospray Ionization. J Proteome Res 2022, 21 (1), 243–249. https://doi.org/10.1021/ACS.JPROTEOME.1C00822.

(29) Han, X.; Gross, R. W. Shotgun Lipidomics: Electrospray Ionization Mass Spectrometric Analysis and Quantitation of Cellular Lipidomes Directly from Crude Extracts of Biological Samples. Mass Spectrom Rev 2005, 24 (3), 367–412. https://doi.org/10.1002/mas.20023.

(30) Javanshad, R.; Venter, A. R. Ambient Ionization Mass Spectrometry: Real-Time, Proximal Sample Processing and Ionization. Analytical Methods 2017, 9 (34), 4896–4907. https://doi.org/10.1039/c7ay00948h.

(31) Unsihuay, D.; Yin, R.; Sanchez, D. M.; Yang, M.; Li, Y.; Sun, X.; Dey, S. K.; Laskin, J. High-Resolution Imaging and Identification of Biomolecules Using Nano-DESI Coupled to Ion Mobility Spectrometry. Anal Chim Acta 2021, 1186, 339085. https://doi.org/10.1016/J.ACA.2021.339085.

(32) Takáts, Z.; Wiseman, J. M.; Gologan, B.; Cooks, R. G. Mass Spectrometry Sampling under Ambient Conditions with Desorption Electrospray Ionization. Science (1979) 2004, 306 (5695), 471–473. https://doi.org/10.1126/SCIENCE.1104404.

(33) Roach, P. J.; Laskin, J.; Laskin, A. Nanospray Desorption Electrospray Ionization : An Ambient Method for Liquid- Extraction Surface Sampling in Mass Spectrometry. Analyst 2010, 135 (9), 2233–2236. https://doi.org/10.1039/C0AN00312C.

(34) Kertesz, V.; Van Berkel, G. J. Liquid Microjunction Surface Sampling Coupled with High-Pressure Liquid Chromatography-Electrospray Ionization-Mass Spectrometry for Analysis of Drugs and Metabolites in Whole-Body Thin Tissue Sections. Anal Chem 2010, 82 (14), 5917–5921. https://doi.org/10.1021/AC100954P.

(35) Eikel, D.; Vavrek, M.; Smith, S.; Bason, C.; Yeh, S.; Korfmacher, W. A.; Henion, J. D. Liquid Extraction Surface Analysis Mass Spectrometry (LESA-MS) as a Novel Profiling Tool for Drug Distribution and Metabolism Analysis: The Terfenadine Example. 2011. https://doi.org/10.1002/rcm.5274.

(36) Otsuka, Y.; Shide, S.; Naito, J.; Kyogaku, M.; Hashimoto, H.; Arakawa, R. Scanning Probe Electrospray Ionization for Ambient Mass Spectrometry. Rapid Communications in Mass Spectrometry 2012, 26 (23), 2725–2732. https://doi.org/10.1002/RCM.6399.

(37) Pan, N.; Rao, W.; Kothapalli, N. R.; Liu, R.; Burgett, A. W. G.; Yang, Z. The Single-Probe: A Miniaturized Multifunctional Device for Single Cell Mass Spectrometry Analysis. Anal Chem 2014, 86 (19), 9376–9380. https://doi.org/10.1021/AC5029038.

(38) Eberlin, L. S.; Ferreira, C. R.; Dill, A. L.; Ifa, D. R.; Cheng, L.; Cooks, R. G. Nondestructive, Histologically Compatible Tissue Imaging by Desorption Electrospray Ionization Mass Spectrometry. ChemBioChem 2011, 12 (14), 2129–2132. https://doi.org/10.1002/cbic.201100411.

(39) Unsihuay, D.; Qiu, J.; Swaroop, S.; Nagornov, K. O.; Kozhinov, A. N.; Tsybin, Y. O.; Kuang, S.; Laskin, J. Imaging of Triglycerides in Tissues Using Nanospray Desorption Electrospray Ionization (Nano-DESI) Mass Spectrometry. Int J Mass Spectrom 2020, 448, 116269. https://doi.org/10.1016/j.ijms.2019.116269.

(40) Weigand, M. R.; Yang, M.; Hu, H.; Zensho, C.; Laskin, J. Enhancement of Lipid Signals with Ammonium Fluoride in Negative Mode Nano-DESI Mass Spectrometry Imaging. Int J Mass Spectrom 2022, 478, 116859. https://doi.org/10.1016/J.IJMS.2022.116859.

(41) Duncan, K. D.; Fang, R.; Yuan, J.; Chu, R. K.; Dey, S. K.; Burnum-Johnson, K. E.; Lanekoff, I. Quantitative Mass Spectrometry Imaging of Prostaglandins as Silver Ion Adducts with Nanospray Desorption Electrospray Ionization. Anal Chem 2018, 90 (12), 7246–7252. https://doi.org/10.1021/acs.analchem.8b00350.

(42) Unsihuay, D.; Su, P.; Hu, H.; Qiu, J.; Kuang, S.; Li, Y.; Sun, X.; Dey, S. K.; Laskin, J. Imaging and Analysis of Isomeric Unsaturated Lipids through Online Photochemical Derivatization of Carbon–Carbon Double Bonds**. Angewandte Chemie International Edition 2021, 60 (14), 7559–7563. https://doi.org/10.1002/ANIE.202016734.

(43) Yin, R.; Burnum-Johnson, K. E.; Sun, X.; Dey, S. K.; Laskin, J. High Spatial Resolution Imaging of Biological Tissues Using Nanospray Desorption Electrospray Ionization Mass Spectrometry. Nature Protocols 2019 14:12 2019, 14 (12), 3445–3470. https://doi.org/10.1038/s41596-019-0237-4.

(44) Yang, M.; Hu, H.; Su, P.; Thomas, P. M.; Camarillo, J. M.; Greer, J. B.; Early, B. P.; Fellers, R. T.; Kelleher, N. L.; Laskin, J. Proteoform-Selective Imaging of Tissues Using Mass Spectrometry**. Angewandte Chemie International Edition 2022, 61 (29), e202200721. https://doi.org/10.1002/ANIE.202200721.

(45) Lanekoff, I.; Thomas, M.; Laskin, J. Shotgun Approach for Quantitative Imaging of Phospholipids Using Nanospray Desorption Electrospray Ionization Mass Spectrometry. Anal Chem 2014, 86 (3), 1872–1880. https://doi.org/10.1021/AC403931R.

(46) Mesa Sanchez, D.; Brown, H. M.; Yin, R.; Chen, B.; Vavrek, M.; Cancilla, M. T.; Zhong, W.; Shyong, B. J.; Zhang, N. R.; Li, F.; Laskin, J. Mass Spectrometry Imaging of Diclofenac and Its Metabolites in Tissues Using Nanospray Desorption Electrospray Ionization. Anal Chim Acta 2022, 1233, 340490. https://doi.org/10.1016/J.ACA.2022.340490.

(47) Drake, R. R.; Powers, T. W.; Norris-Caneda, K.; Mehta, A. S.; Angel, P. M. In Situ Imaging of N-Glycans by MALDI Imaging Mass Spectrometry of Fresh or Formalin-Fixed Paraffin-Embedded Tissue. Curr Protoc Protein Sci 2018, 94 (1), e68. https://doi.org/10.1002/CPPS.68.

(48) Nguyen, S. N.; Sontag, R. L.; Carson, J. P.; Corley, R. A.; Ansong, C.; Laskin, J. Towards High-Resolution Tissue Imaging Using Nanospray Desorption Electrospray Ionization Mass Spectrometry Coupled to Shear Force

Microscopy. J Am Soc Mass Spectrom 2018, 29 (2), 316–322. https://doi.org/10.1007/s13361-017-1750-8.

(49) Lanekoff, I.; Heath, B. S.; Liyu, A.; Thomas, M.; Carson, J. P.; Laskin, J. Automated Platform for High-Resolution Tissue Imaging Using Nanospray Desorption Electrospray Ionization Mass Spectrometry. Anal Chem 2012, 84 (19), 8351–8356. https://doi.org/10.1021/ac301909a.

(50) Yin, R.; Kyle, J.; Burnum-Johnson, K.; Bloodsworth, K. J.; Sussel, L.; Ansong, C.; Laskin, J. High Spatial Resolution Imaging of Mouse Pancreatic Islets Using Nanospray Desorption Electrospray Ionization Mass Spectrometry. Anal Chem 2018, 90 (11), 6548–6555. https://doi.org/10.1021/acs.analchem.8b00161.

(51) Huffstutler, C. D.; Sanchez, D. M.; Weigand, M. R.; Hu, H.; Li, X.; Chegwidden, A. J.; Nagornov, K. O.; Kozhinov, A. N.; Tsybin, Y. O.; Laskin, J. Multiple Selected Ion Monitoring Mode for Sensitive Imaging of Eicosanoids in Tissues Using Nanospray Desorption Electrospray Ionization (Nano-DESI) Mass Spectrometry. Int J Mass Spectrom 2023, 491, 117101. https://doi.org/10.1016/J.IJMS.2023.117101.

(52) Kalmar, J. G.; Garrard, K. P.; Muddiman, D. C. GlycoHunter: An Open-Source Software for the Detection and Relative Quantification of INLIGHT-Labeled N-Linked Glycans. J Proteome Res 2021, 20 (4), 1855–1863. https://doi.org/10.1021/ACS.JPROTEOME.0C00840.

(53) Cooper, C. A.; Gasteiger, E.; Packer, N. H. GlycoMod - A Software Tool for Determining Glycosylation Compositions from Mass Spectrometric Data. Proteomics (Weinheim) 2001, 1 (2), 340–349. https://doi.org/10.1002/1615-9861(200102)1:2<340::AID-PROT340>3.0.CO;2-B.

(54) Alocci, D.; Mariethoz, J.; Gastaldello, A.; Gasteiger, E.; Karlsson, N. G.; Kolarich, D.; Packer, N. H.; Lisacek, F. GlyConnect: Glycoproteomics Goes Visual, Interactive, and Analytical. J Proteome Res 2019, 18 (2), 664–677. https://doi.org/10.1021/ACS.JPROTEOME.8B00766.

(55) Ceroni, A.; Maass, K.; Geyer, H.; Geyer, R.; Dell, A.; Haslam, S. M. GlycoWorkbench: A Tool for the Computer-Assisted Annotation of Mass Spectra of Glycans. J Proteome Res 2008, 7 (4), 1650–1659. https://doi.org/10.1021/PR7008252.

(56) West, C. A.; Wang, M.; Herrera, H.; Liang, H.; Black, A.; Angel, P. M.; Drake, R. R.; Mehta, A. S. N-Linked Glycan Branching and Fucosylation Are Increased Directly in Hcc Tissue As Determined through in Situ Glycan Imaging. J Proteome Res 2018, 17 (10), 3454–3462. https://doi.org/10.1021/ACS.JPROTEOME.8B00323.

(57) Ochoa-Rios, S.; Blaschke, C. R. K.; Wang, M.; Peterson, K. D.; DelaCourt, A.; Grauzam, S. E.; Lewin, D.; Angel, P.; Roberts, L. R.; Drake, R.; Mehta, A. S. Analysis of N-Linked Glycan Alterations in Tissue and Serum Reveals Promising Biomarkers for Intrahepatic Cholangiocarcinoma. Cancer research communications 2023, 3 (3), 383–394. https://doi.org/10.1158/2767-9764.CRC-22-0422.

(58) DelaCourt, A.; Black, A.; Angel, P.; Drake, R.; Hoshida, Y.; Singal, A.; Lewin, D.; Taouli, B.; Lewis, S.; Schwarz, M.; Isabel Fiel, M.; Mehta, A. S. N-Glycosylation Patterns Correlate with Hepatocellular Carcinoma Genetic Subtypes. Mol Cancer Res 2021, 19 (11), 1868. https://doi.org/10.1158/1541-7786.MCR-21-0348.

(59) Llovet, J. M.; Kelley, R. K.; Villanueva, A.; Singal, A. G.; Pikarsky, E.; Roayaie, S.; Lencioni, R.; Koike, K.; Zucman-Rossi, J.; Finn, R. S. Hepatocellular Carcinoma. Nature Reviews Disease Primers 2021 7:1 2021, 7 (1), 1–28. https://doi.org/10.1038/s41572-020-00240-3.

(60) Zhang, H.; Zhang, W.; Jiang, L.; Chen, Y. Recent Advances in Systemic Therapy for Hepatocellular Carcinoma. Biomark Res 2022, 10 (1), 1–21. https://doi.org/10.1186/S40364-021-00350-4.

(61) Mesa Sanchez, D.; Brown, H. M.; Yin, R.; Chen, B.; Vavrek, M.; Cancilla, M. T.; Zhong, W.; Shyong, B. J.; Zhang, N. R.; Li, F.; Laskin, J. Mass Spectrometry Imaging of Diclofenac and Its Metabolites in Tissues Using Nanospray Desorption Electrospray Ionization. Anal Chim Acta 2022, 1233, 340490. https://doi.org/10.1016/J.ACA.2022.340490.

(62) Clift, C. L.; Mehta, A.; Drake, R. R.; Angel, P. M. Multiplexed Imaging Mass Spectrometry of Histological Staining, N-Glycan and Extracellular Matrix from One Tissue Section: A Tool for Fibrosis Research. Methods in Molecular Biology 2021, 2350, 313–329. https://doi.org/10.1007/978-1-0716-1593-5_20.

(63) Powers, T. W.; Holst, S.; Wuhrer, M.; Mehta, A. S.; Drake, R. R. Two-Dimensional N-Glycan Distribution Mapping of Hepatocellular Carcinoma Tissues by MALDI-Imaging Mass Spectrometry. Biomolecules 2015, 5 (4), 2554–2572. https://doi.org/10.3390/BIOM5042554.

(64) Blaschke, C. R. K.; Hartig, J. P.; Grimsley, G.; Liu, L.; Semmes, O. J.; Wu, J. D.; Ippolito, J. E.; Hughes-Halbert, C.; Nyalwidhe, J. O.; Drake, R. R. Direct N-Glycosylation Profiling of Urine and Prostatic Fluid Glycoproteins and Extracellular Vesicles. Front Chem 2021, 9 (September), 1–12. https://doi.org/10.3389/fchem.2021.734280.

(65) Drake, R. R.; Jones, E. E.; Powers, T. W.; Nyalwidhe, J. O. Altered Glycosylation in Prostate Cancer. Adv Cancer Res 2015, 126, 345–382. https://doi.org/10.1016/BS.ACR.2014.12.001.

(66) Domon, B.; Costello, C. E. A Systematic Nomenclature for Carbohydrate Fragmentations in FAB-MS/MS Spectra of Glycoconjugates. Glycoconjugate Journal 1988 5:4 1988, 5 (4), 397–409. https://doi.org/10.1007/BF01049915.

(67) Wong, H. T. K.; Chen, X.; Wu, R.; Wong, Y. L. E.; Hung, Y. L. W.; Chan, T. W. D. Dissociation of Mannose-Rich Glycans Using Collision-Based and Electron-Based Ion Activation Methods. J Am Soc Mass Spectrom 2022, 33 (5), 803–812. https://doi.org/10.1021/JASMS.1C00385.